

# Unraveling spin texture and spin-orbit coupling contributions in spin triplet superconductivity

Pablo Tuero<sup>†,1</sup>, César González-Ruano<sup>†,1</sup>, Yuan Lu,<sup>2</sup> Coriolan Tiusan,<sup>2,3</sup> and Farkhad G. Aliev<sup>1,\*</sup>

<sup>1</sup>*Departamento de Física de la Materia Condensada C-III,  
Universidad Autónoma de Madrid, Madrid 28049, Spain*

<sup>2</sup>*Institut Jean Lamour, Nancy Université, 54506 Vandoeuvre-les-Nancy Cedex, France*

<sup>3</sup>*Department of Solid State Physics and Advanced Technologies,  
Faculty of Physics, Babes-Bolyai University, Cluj Napoca 400114, Romania*

<sup>†</sup>*Equally contributing authors*

Over the past decade, it has been proposed theoretically and confirmed experimentally that long-range spin triplet (LRT) superconductivity can be generated in ferromagnet-superconductor hybrids either by the presence of spin textures (ST-LRT) or thanks to spin-orbit coupling (SOC-LRT). Nevertheless, there has been no theoretical or experimental investigation to date suggesting that both contributions could simultaneously exist within an experimental system. To disentangle these contributions, we present a comprehensive study of superconducting quasiparticle interference effects taking place inside a ferromagnetic layer interfacing a superconductor, through the investigation of above-gap conductance anomalies (CAs) related to MacMillan-Rowell resonances. The bias dependence of the CAs has been studied under a wide range of in-plane (IP) and out-of-plane (OOP) magnetic fields in two types of epitaxial, V/MgO/Fe-based ferromagnet-superconductor junctions with interfacial spin-orbit coupling. We observe an anisotropy of the CAs amplitude under small IP and OOP magnetic fields while remaining weakly affected by high fields, and implement micro-magnetic simulations to help us distinguish between the ST-LRT and SOC-LRT contributions. Our findings suggest that further exploration of Fabry-Pérot type interference effects in electron transport could yield valuable insights into the hybridization between superconductors and ferromagnets induced by spin-orbit coupling and spin textures.

## I. INTRODUCTION

For more than a decade, the conversion of “conventional” singlet Cooper pairs to equal-spin triplet pairs in superconductor/ferromagnet (S/F) interfaces has been linked with inhomogeneous magnetism or spin textures (STs)<sup>1-3</sup>. This was the foundation for the development of new energy-efficient devices and, in particular, dissipationless cryogenic memories<sup>4</sup>, whose operation rules are based on superconducting spintronics<sup>4,5</sup>. Well before these developments, Gorkov and Rashba<sup>7</sup> pointed out that singlet and triplet Cooper pair mixing could also be created by interfacial spin-orbit coupling (SOC) at the surface of a superconducting layer. More recently, a number of theoretical papers showed that, in S/F heterostructures, SOC could provide singlet to equal-spin triplet pair conversion<sup>8-10</sup>, potentially producing long-range triplet (LRT) proximity effects, which was later confirmed experimentally<sup>3,11,13-16</sup>. Importantly, some studies suggest that SOC can also be synthesized by moving electrons in inhomogeneous magnetic fields<sup>17</sup> or through localized STs<sup>18,19</sup>, opening an alternative route to engineer hybrid quantum devices.

In clean S/F hybrids, Fabry-Pérot interferences due to electron confinement can result in the so-called MacMillan-Rowell resonances (MRRs)<sup>2,20,21</sup>, originated as two Andreev-type and two normal reflections take place inside the ferromagnetic electrode interfacing the superconductor<sup>7,23,25,26</sup>. Tomasch resonances<sup>27</sup> (TRs)

are similar interference phenomena occurring in the superconducting layer that have been recently put forward to be a probe to distinguish between conventional and topological superconductivity<sup>28</sup>. The above-gap conductance anomalies (CAs) originated by these two processes were suggested as an unequivocal experimental proof for equal-spin triplet formation in S/F heterostructures<sup>7</sup>. The full suppression of these CAs under large external magnetic fields pointed towards a direct link between LRT generation and spin textures<sup>8</sup>.

Recently, epitaxial V/MgO/Fe heterostructures have been proposed as an example of a S/F system coupled by interfacial SOC<sup>3,13,14</sup>. These superconductor-ferromagnet hybrids showed experimental evidence for SOC-induced spin-triplet pairing, observed through the sub-gap conductance anisotropy, above-gap CAs in remanent magnetization states, and superconductivity induced change of the magneto-crystalline anisotropy<sup>3,13,14</sup>. In this system, Rashba SOC at the Fe/MgO interface causes perpendicular magnetic anisotropy (PMA) in the interfacial atomic layers<sup>30</sup>, which competes with the in-plane shape anisotropy<sup>31</sup> potentially inducing interfacial spin textures. For this reason, one could expect that, in V/MgO/Fe-based junctions, both SOC and STs could contribute to spin-triplet Cooper pair formation at relatively low magnetic fields.

In this Letter, we demonstrate that studying the anisotropy of MRR-induced CAs in S/F junctions under in-plane (IP) and out-of-plane (OOP) applied mag-

arXiv:2403.02819v1 [cond-mat.supr-con] 5 Mar 2024

netic fields provides a unique tool to disentangle the STs and SOC contributions to spin-triplet superconductivity. Our analysis is based on the consideration that SOC-induced LRTs (SOC-LRTs) should be more robust to magnetic field than those induced by spin textures (ST-LRTs), which should strongly diminish under a high field saturating the magnetization. We find that, in contrast to previous studies<sup>8</sup>, the CAs in our V/MgO/Fe-based junctions remain mostly unaffected under high applied fields, firmly pointing towards SOC-LRTs. However, at low magnetic fields (where more STs are present) the amplitude of the CAs strongly depends on the magnetic field direction. Our experimental observations are qualitatively supported by micromagnetic simulations pointing towards the anisotropic induction of spin textures in the Fe layer under low IP and OOP magnetic fields.

## II. RESULTS AND DISCUSSION

Figure 1a-b sketches the two types of samples under study. The structure of the S/F/F junctions is V(40 nm)/MgO(2 nm)/Fe(10 nm)/MgO(2 nm)/Fe(10 nm)/Co(20 nm), while the structure of the F/S/F ones is Fe(45 nm)/MgO(2 nm)/V(40 nm)/MgO(2 nm)/Fe(10 nm)/Co(20 nm). In both cases V is the superconducting electrode, with a critical temperature ( $T_C$ ) of about 4 K; the MgO/Fe interface provides symmetry filtering<sup>32</sup>, high spin polarization, and interfacial SOC<sup>33</sup>; and Fe and Fe/Co are the soft and hard ferromagnetic layers respectively. They were epitaxially grown by MBE and controlled by in-situ RHEED, as described in refs.<sup>32,33</sup> and the supplemental material. Figure 1c-d illustrates the MacMillan reflections in the absence (c) or presence (d) of spin flips, induced by interfacial STs and/or SOC.

Figure 2 shows that the conductance curves of S/F/F junctions (measured at  $T = 0.3$  K =  $0.075T_C$  unless otherwise stated) present several above-gap CAs which appear to have a periodicity with applied bias (see the inset in Figure 2a). As mentioned above, this kind of CAs have been linked to MacMillan and Tomasch reflections<sup>3,7</sup> generating LRTs in S/F systems with highly polarized ferromagnets. However, the observed periodicity of the CAs suggests that MRRs are the leading order interference mechanism, since these reflections, depicted in Figure 1c-d, give rise to conductance oscillations at periodic characteristic bias:

$$V_n = V_0 + nhv_F^{\text{Fe}}/4t_{\text{Fe}}, \quad (1)$$

where  $n = 0, 1, 2, \dots$  label the successive conductance oscillation peaks,  $h$  is the Planck constant,  $v_F^{\text{Fe}}$  is the Fermi velocity in the layer where the interference process takes place (in our case, the soft Fe layer), and  $t_{\text{Fe}}$

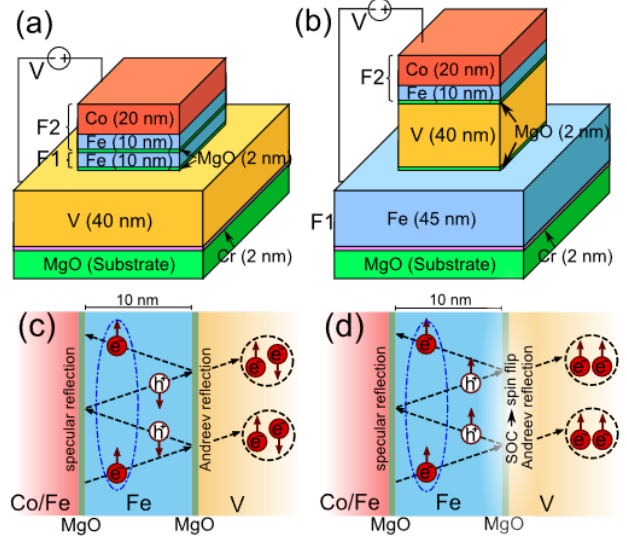


FIG. 1: Sketch of the S/F/F (a) and F/S/F (b) junctions, showing the disposition and thickness of each layer in the structure. The lateral sizes range from  $10 \times 10$  to  $30 \times 30 \mu\text{m}^2$  (samples with a larger area tend to not show such clear CAs due to interference averaging). (c) conventional MRR, while (d) is the MRR with spin-flip, allowed in the V/MgO/Fe system thanks to interfacial SOC. The whole process is as follows: An electron in the F layer (lower part of the sketches) undergoes Andreev reflection as a hole at the interface. The reflected hole propagates to the opposite interface and is again reflected there (with a normal reflection process). It then travels back to the F/S interface and undergoes another Andreev reflection, turning again into an electron with the same spin as the initial one (upper part). Here is where the interference phenomenon takes place with the initial electron (the two electrons are circled in blue), which in turn produces the observed CAs.

its thickness (10 nm in our S/F/F junctions and 45 nm in the F/S/F ones). For MRRs to occur, the gap-induced phase coherence between the initial electron and the reflected hole is maintained through the whole path back and forth the F layer (a total distance of at least 40 nm and 180 nm for the S/F/F and F/S/F junctions respectively). This is a strong hint of long-range superconducting proximity effects, as it means that superconducting correlations must survive deep into the Fe layer.

Importantly, Figure 2b shows how the CAs emerge mainly below  $T_C$  (see the supplemental material for a detailed explanation of the CAs analysis methods). Despite this, we don't completely exclude that normal electron interference processes could also have some residual contribution. These could naturally emerge in fully epitaxial junctions due to the electron confinement (i.e. resonance transmission<sup>34</sup>) in the Fe layer, situated between two thin MgO layers acting as symmetry filters due to

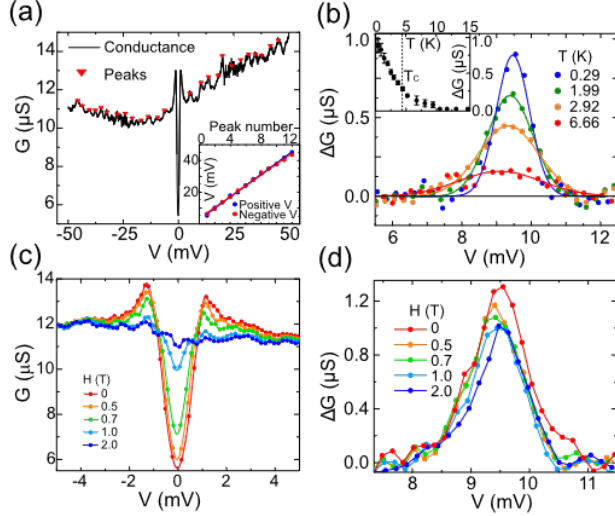


FIG. 2: (a) Periodic CAs observed in a  $20 \times 20 \mu\text{m}^2$  S/F/F sample, with red markers over each peak detected. Inset: periodicity analysis, showing peak bias vs peak number for the positive (blue) and negative (red) bias ranges with linear fits. (b) Amplitude ( $\Delta G$  above the baseline conductance) of one of the CAs for different temperatures, from below to above  $T_C$  ( $\sim 4$  K). The inset plots the amplitude of the peak above the base level vs temperature. The critical temperature is marked with a vertical dashed line. (c) Conductance of the sample vs applied bias around the superconducting gap for different IP applied magnetic fields, showing how it disappears under an applied field of  $H = 2$  T. (d) The same peak analyzed in panel (b) remains visible under high IP applied fields, even above the magnitude that suppresses the superconducting gap in the previous panel.

“hot spots” with enhanced electronic transmission for specific  $k$  values<sup>35</sup>. Overall, the clear observation of CAs is indicative of the smoothness of the interfaces in the junctions ensured by the layer-by-layer epitaxial growth monitored by in-situ electron diffraction, which allows for the observation of quasiparticle interference effects. An extended discussion about the analysis of the CAs based on equation 1, as well as different processes that could be contributing to the conductance features in our junctions (including the above-mentioned Tomasch resonances), is given in the supplemental material.

In order to get deeper insight from the CAs, both the sub-gap conductance and one of the CAs in an S/F/F junction are thoroughly studied as a function of magnetic field in Figure 2c-d. Remarkably, these figures show how the superconducting gap is suppressed by an IP magnetic field of about 2 T, while the CAs remain almost unaffected by the same field.

The combination of these observations has several implications: First, the CAs are linked with the emergence of superconductivity, since they nearly disappear above

$T_C$  as seen in Fig. 2b. Second, the fact that the CA are robust under high applied fields that suppress the superconducting gap implies that they can’t be the result of singlet superconductivity, since a singlet Cooper pair with anti-parallel spins would be destroyed by such fields<sup>36</sup>. Therefore, they are most likely related to triplet superconductivity, and in particular equal-spin triplet Cooper pairs, which can survive high magnetic fields and inside a ferromagnet. Finally, the robustness of the CAs to high fields also implies that these LRTs shouldn’t be exclusively produced by spin textures, as these would also be destroyed by a high applied field that fully saturates the Fe layer. Instead, we argue that the Rashba SOC at the MgO/Fe interface is the main responsible for the CAs, which nonetheless could be enhanced by an extra contribution from spin textures.

To investigate the possible contribution of spin textures to the CAs and LRT formation, we have analyzed the response of the CAs to the magnetic field direction, in a field range not yet saturating the Fe layer magnetization. Figure 3a shows a  $G(V)$  curve around a CA peak of another S/F/F junction at  $T = 0.3$  K after the background conductance is subtracted. This CA persisted for fields up to  $H_{IP} = 2$  T and  $H_{OOP} = 0.7$  T, again exceeding the critical field which suppresses the superconducting gap. The dependence of the CA amplitude with IP and OOP applied fields is presented in Fig. 3b. The CA amplitude remains approximately constant for an IP magnetic field up to 2 T, in qualitative agreement with experiments on smaller junctions. Surprisingly, when an OOP field is applied, the CA amplitude is first enhanced with respect to the IP base level. The maximum amplitude is reached for  $H_{OOP} \approx 0.3$  T, and further increasing the OOP field up to 7 kOe removes the observed CA excess.

To understand these results, we consider the possible role of PMA-induced interfacial spin textures at the MgO/Fe interface, which is sketched in Figure 3c. It is well known that the PMA present at the MgO/Fe interfaces provides perpendicular room temperature magnetization in MgO/Fe(2 nm) films<sup>37,38</sup>. In our view, the CA amplitude under IP field gives a baseline for the spin-triplet generation rate via SOC, as the magnetization of the Fe layer in this situation is nearly fully saturated thanks to the dominating IP anisotropy. By contrast, when a low  $H_{OOP}$  is applied, the Fe atomic layers closest to the surface tend to align with this field due to the PMA, increasing the angle  $\phi$  with the IP direction. The presence of these spin textures or non-collinearity close to the MgO/Fe interface could then open an additional channel for LRT generation<sup>3,39,40</sup>, which in turn would enhance the CA amplitude. However, if the OOP field is further increased, the inner layers of Fe (which were initially oriented IP) would also align with the OOP magnetic field, removing the STs (therefore reducing the angle gradient  $\Delta\phi$ ) and letting the V/MgO/Fe system

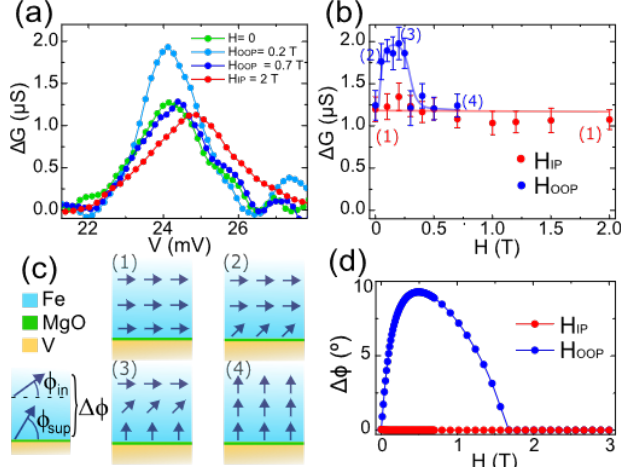


FIG. 3: (a)  $\Delta G(V)$  of a CA for different IP and OOP applied fields in a  $30 \times 30 \mu\text{m}^2$  S/F/F junction after subtracting the background conductance. (b) Amplitude of the same CA versus applied IP and OOP fields. Error bars mark the 95% confidence bounds. The lines are guides for the eye. The numbers within the graph correspond to the different parts in panel (c), where we sketch the proposed magnetization configuration during these experiments and define the interfacial magnetization gradient (spin texture)  $\Delta\phi$  simulated in the next panel. (1) After an initial saturation with an IP field of 0.3 T, the magnetization is homogeneous. (2) A small OOP applied field starts inducing an angle gradient in the surface layers due to the PMA. (3) as the OOP field increases, the angle gradient reaches a maximum between the surface and inner layers. (4) a large enough OOP field saturates the magnetization, returning the sample to a reduced interfacial spin gradient configuration. (d) Dependence of the interfacial spin gradient  $\Delta\phi$  vs IP and OOP applied field obtained from micromagnetic simulations. The supplemental material provides details about the parameters used in the simulations.

again only with the interfacial SOC contribution to LRT formation.

This scenario is qualitatively supported by the results of micromagnetic simulations shown in Figure 3d, where we study the evolution of spin textures in a 10 nm thick Fe layer under IP and OOP applied fields. The simulations (see the supplemental material for details about the system and parameters used) show that, while an IP field or a large OOP field quickly saturates the magnetization, a moderate OOP field can initially maximize the angle between the magnetization of the atomic layers interfacing the MgO (where PMA is present) and the inner layers where the IP shape anisotropy dominates ( $\Delta\phi$  shown in Figure 3d, the definition is sketched in Figure 3c). These interfacial STs could open the channel for ST-LRT generation, accounting for the CA enhancement under low OOP fields.

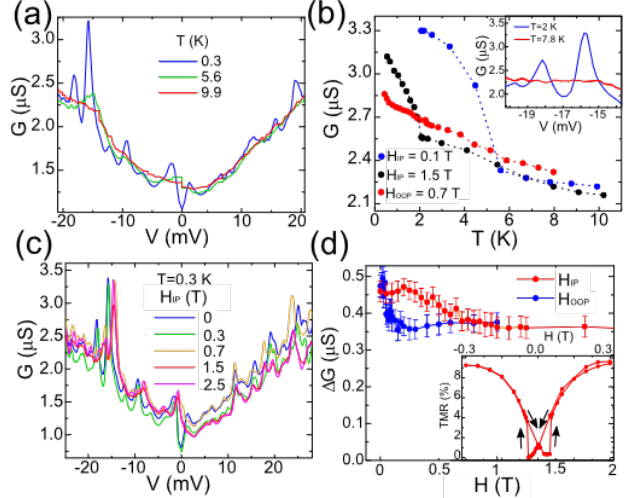


FIG. 4: CAs in a F/S/F junction. (a) Conductance curves vs applied bias of a typical F/S/F junction below (blue), near (green), and above (red) the superconducting critical temperature, showing how the CAs disappear in the normal state. (b) Maximum conductance of a selected CA near  $-15$  mV vs temperature for different applied magnetic fields, both IP and OOP. The black dashed vertical line marks the critical temperature. The lines are guides for the eyes. The inset shows the conductance around the same CA below and above  $T_C$ . (c) Conductance vs applied bias of the same junction, at  $T = 0.3$  K and for different IP applied fields, showing the robustness of the CAs under large magnetic fields. (d) Amplitude of a CA vs applied field, both IP and OOP. The inset shows an IP magnetoresistance measured at  $T = 0.3$  K, showing that the IP magnetization doesn't fully saturate until an applied field of about 0.3 T.

We also observed similar CAs in F/S/F junctions (the structure of these samples is sketched in Figure 1b), as shown in Figure 4, where the conductance oscillations found in one of these junctions are studied under different temperatures and applied magnetic fields. Here, the Fe electrode is surrounded by the substrate MgO/Cr from one side and the MgO barrier from the other one. Having in view that the Cr behaves as a symmetry-dependent metallic barrier in fully epitaxial MgO-based magnetic tunnel junctions<sup>41</sup>, this Fe electrode layer will be equivalent to the 10 nm Fe layer in the S/F/F junctions. The CAs in these junctions are also robust under high applied magnetic fields, and are nearly destroyed above  $T_C$  (which is slightly higher on these junctions compared to the S/F/F ones, see Figure 4b), so they are also the result of Fabry-Pérot-like interference effects in the presence of STs and SOC. However, Figure 4d shows that the behavior of the CAs in an F/S/F junction is in some ways different to the one previously discussed in an S/F/F one. While in both types of junctions the CAs maintain a baseline level in the high field regime,

in the F/S/F ones the CA enhancement at low fields is seen both for IP and OOP fields.

We explain these differences by the influence of a much stronger anti-parallel coupling in the F/S/F junctions compared to the S/F/F ones, which could induce additional spin textures in the low IP field regime. Combined with the PMA in the atomic layers near the MgO barrier, this results in the magnetization only becoming fully saturated under an IP applied field above 0.3 T (see Figure 4d inset, showing an IP magnetoresistance). In contrast, this extra amplitude of the CAs disappears more quickly with an OOP applied field, as in this case the PMA and the applied field point in the same direction, resulting in the magnetization being already fully saturated under a lower OOP field. As observed in the S/F/F junctions, the CAs persist in the high field regime, supporting a scenario of dominant SOC-induced LRT pair generation with an additional contribution of ST-LRTs in the low field regime.

### III. CONCLUSIONS

In summary, our Letter demonstrates the capability to distinguish between the intrinsic (SOC) and extrinsic (spin textures) contributions to spin-triplet Cooper pair formation in superconductor-ferromagnet junctions. The method is based on the direct link<sup>3,7,26</sup> already established between the emergence of periodic conductance anomalies, produced by quasiparticle interference

within the ferromagnetic layer, and long-range equal spin triplet superconductivity. The anisotropic response of the CAs under different directions and magnitudes of external magnetic fields allowed us to discriminate between the two main mechanisms previously suggested to be responsible for LRT generation. Our findings call for more fundamental studies of quasiparticle interference in hybrid superconducting nanoscale systems, where superconducting correlations could be altered by the coupling of the spin and orbital motion of electrons.

### Acknowledgements

Authors thank Jacob Linder for discussions and Isidoro Martinez for help with the samples characterization. The work in Madrid was supported by Spanish Ministry of Science and Innovation (PID2021-124585NB-C32 and TED2021-130196B-C22). F.G.A. also acknowledges financial support from the Spanish Ministry of Science and Innovation through the María de Maeztu Programme for Units of Excellence in R&D (CEX2018-000805-M) and “Acción financiada por la Comunidad de Madrid en el marco del convenio plurianual con la Universidad Autónoma de Madrid en Línea 3: Excelencia para el Profesorado Universitario”. C. T. acknowledges the UEFISCDI project “MODESKY” ID PN-III-P4-ID- 880 PCE-2020-0230-P, grant No. UEFISCDI: PCE 245/02.11.2021.

---

\* e-mail: farkhad.aliev@uam.es

- <sup>1</sup> R. S. Keizer, S. T. B. Goennenwein, T. M. Klapwijk, G. Miao, G. Xiao, and A. A. Gupta, Spin Triplet Supercurrent through the Half-Metallic Ferromagnet CrO<sub>2</sub>, *Nature* **439**, 825 (2006).
- <sup>2</sup> T. S. Khaire, M. A. Khasawneh, W. P. Pratt, Jr. and N. O. Birge, Observation of Spin-Triplet Superconductivity in Co-Based Josephson Junctions, *Phys. Rev. Lett.* **104**, 137002 (2010).
- <sup>3</sup> J. W. A. Robinson, J. D. S. Witt, M. G. Blamire, Controlled Injection of Spin-Triplet Supercurrents into a Strong Ferromagnet, *Science* **329**, 59 (2010).
- <sup>4</sup> N. O. Birge and M. Houzet, Spin-Singlet and Spin-Triplet Josephson Junctions for Cryogenic Memory, *IEEE Magnetics Letters*, **10**, 4509605, 1-5 (2019).
- <sup>5</sup> J. Linder and J. W. A. Robinson, Superconducting spintronics, *Nature Physics* **11**, 307-315 (2015).
- <sup>6</sup> M. Eschrig, Spin-polarized supercurrents for spintronics: a review of current progress, *Rep. Prog. Phys.* **78**, 104501 (2015).
- <sup>7</sup> L. P. Gorkov and E. I. Rashba, Superconducting 2D System with Lifted Spin Degeneracy Mixed Singlet-Triplet State, *Phys. Rev. Lett.* **87**, 037004 (2001).
- <sup>8</sup> F. S. Bergeret and I. V. Tokatly, Singlet-Triplet Conversion and the Long-Range Proximity Effect in Superconductor-

- Ferromagnet Structures with Generic Spin Dependent Fields, *Phys. Rev. Lett.* **110**, 117003 (2013).
- <sup>9</sup> F. S. Bergeret and I. V. Tokatly, Spin-orbit coupling as a source of long-range triplet proximity effect in superconductor-ferromagnet hybrid structures, *Phys. Rev. B* **89**, 134517 (2014).
- <sup>10</sup> S. H. Jacobsen, J. A. Ouassou and J. Linder, Critical temperature and tunneling spectroscopy of superconductor-ferromagnet hybrids with intrinsic Rashba-Dresselhaus spin-orbit coupling, *Phys. Rev. B* **92**, 024510 (2015).
- <sup>11</sup> N. Banerjee, J. A. Ouassou, Y. Zhu, N. A. Stelmashenko, J. Linder and M. G. Blamire, Controlling the superconducting transition by spin-orbit coupling, *Phys. Rev. B* **97**, 184521 (2018).
- <sup>12</sup> I. Martínez, P. Högl, C. González-Ruano, J. P. Cascales, C. Tiusan, Y. Lu, M. Hehn, A. Matos-Abiague, J. Fabian, I. Zutic and F. G. Aliev, Interfacial Spin-Orbit Coupling: A Platform for Superconducting Spintronics, *Phys. Rev. Applied* **13**, 014030 (2020).
- <sup>13</sup> C. González-Ruano, D. Caso, L. G. Johnsen, C. Tiusan, M. Hehn, N. Banerjee, J. Linder and Farkhad G. Aliev, Superconductivity-induced change in magnetic anisotropy in epitaxial ferromagnet-superconductor hybrids with spin-orbit interaction, *Phys. Rev. B* **102**, 020405(R) (2020).
- <sup>14</sup> C. González-Ruano, D. Caso, L. G. Johnsen, C. Tiusan,

- M. Hehn, N. Banerjee, J. Linder and Farkhad G. Aliev, Superconductivity assisted change of the perpendicular magnetic anisotropy in V/MgO/Fe junctions, *Scientific Reports* **11**, 19041 (2021).
- <sup>15</sup> K-R. Jeon et. al., Tunable Pure Spin Supercurrents and the Demonstration of Their Gateability in a Spin-Wave Device, *Phys. Rev. X* **10**, 031020 (2020).
- <sup>16</sup> R. Cai et. al., Evidence for anisotropic spin-triplet Andreev reflection at the 2D van der Waals ferromagnet/superconductor interface, *Nat. Comm.* **12**, 6725 (2021).
- <sup>17</sup> S.I. Pekar and G.I. Rashba, Combined Resonance in Crystals in Inhomogeneous Magnetic Fields, *JETP* **20**, 5, 1295 (1964).
- <sup>18</sup> M. M. Desjardins, L. C. Contamin, M. R. Delbecq, M. C. Dartailh, L. E. Bruhat, T. Cubaynes, J. J. Viennot, F. Mallet, S. Rohart, A. Thiaville, A. Cottet and T. Kontos, Synthetic spin-orbit interaction for Majorana devices, *Nat. Mat* **18**, 1060–1064 (2019).
- <sup>19</sup> N. Davier and R. Ramazashvili, Texture-induced spin-orbit coupling and skyrmion-electron bound states in a Néel antiferromagnet, *Phys. Rev. B* **107**, 01440607 (2023).
- <sup>20</sup> J. M. Rowell and W. L. McMillan, Electron interference in a normal metal induced by superconducting contacts. *Phys. Rev. Lett.* **16**, 453–456 (1966).
- <sup>21</sup> J. M. Rowell, Tunneling observation of bound states in a normal metal-superconductor sandwich. *Phys. Rev. Lett.* **30**, 167–170 (1973).
- <sup>22</sup> W. L. McMillan and P. W. Anderson, Theory of geometrical resonances in the tunneling characteristics of thick films of superconductors, *Phys. Rev. Lett.* **16**, 85–87 (1966).
- <sup>23</sup> M. J. M. de Jong and C. W. J. Beenakker, Andreev Reflection in Ferromagnet-Superconductor Junctions, *Physical Review Letters* **74**, 1657 (1995).
- <sup>24</sup> C. Visani, Z. Sefrioui, J. Tornos, C. Leon, J. Briatico, M. Bibes, A. Barthélémy, J. Santamaría and J. E. Villegas, Equal-spin Andreev reflection and long-range coherent transport in high-temperature superconductor/half-metallic ferromagnet junctions *Nature Physics* **8**, 539–543 (2012).
- <sup>25</sup> A. S. Mel'nikov, A. V. Samokhvalov, S. M. Kuznetsova, and A. I. Buzdin, Interference Phenomena and Long-Range Proximity Effect in Clean Superconductor-Ferromagnet Systems, *Phys. Rev. Lett.* **109**, 237006 (2012).
- <sup>26</sup> C. Visani, A. Costa, M. Sutula, V. Lauter, J. Song, J. Fabian and J. S. Moodera, Signatures of superconducting triplet pairing in Ni-Ga bilayer junctions *New J. Phys.* **24** 033046 (2022).
- <sup>27</sup> W. J. Tomasch, Geometrical Resonance in the Tunneling Characteristics of Superconducting Pb, *Phys. Rev. Lett.* **15**, 672 (1965).
- <sup>28</sup> A. Strkalj, X-R. Chen, W. Chen, D. Y. Xing and O. Zilberberg, Tomasch Oscillations as Above-Gap Signature of Topological Superconductivity, *Phys. Rev. Lett.* **132**, 066301 (2024).
- <sup>29</sup> C. Visani, F. Cuellar, A. Pérez-Muñoz, Z. Sefrioui, C. León, J. Santamaría and J. E. Villegas, Magnetic field influence on the proximity effect at YBa<sub>2</sub>Cu<sub>3</sub>O<sub>7</sub>/La<sub>2/3</sub>Ca<sub>1/3</sub>MnO<sub>3</sub> superconductor/half-metal *Phys. Rev. B* **92**, 014519 (2015).
- <sup>30</sup> B. Dieny and M. Chshiev, Perpendicular magnetic anisotropy at transition metal/oxide interfaces and applications, *Rev. Mod. Phys.* **89**, 025008 (2017).
- <sup>31</sup> I. Martínez, C. Tiusan, M. Hehn, M. Chshiev and F. G. Aliev, Symmetry broken spin reorientation transition in epitaxial MgO/Fe/MgO layers with competing anisotropies, *Sci. Rep.* **8**, 9463 (2018).
- <sup>32</sup> C. Tiusan, M. Hehn, F. Montaigne, F. Greullet, S. Andrieu and A. Schuhl, Spin tunneling phenomena in single crystal magnetic tunnel junction systems, *J. Phys.: Condens. Matter* **19**, 165201 (2007).
- <sup>33</sup> Y. Lu, H. X. Yang, C. Tiusan, M. Hehn, M. Chshiev, C. Bellouard, B. Kierren, G. Lengaigne, A. Duluard, D. Lacour and F. Montaigne, Spin-orbit coupling effect by minority interface resonance states in single-crystal magnetic tunnel junctions, *Phys. Rev. B* **86**, 184420 (2012)
- <sup>34</sup> L. Ferrari, I. Grimaldi, P. M. Sheverdyayeva, Asish K. Kundu, P. Moras, M. Papagno, C. Carbone and D. Pacile, Electron Confinement Effects in Silver Films Embedded between Graphene and Metallic Substrates *J. Phys. Chem. C*, **123**, 15, 9764–9769 (2019).
- <sup>35</sup> W. H. Butler, X.-G. Zhang, T. C. Schulthess, and J. M. MacLaren, Spin-dependent tunneling conductance of Fe—MgO—Fe sandwiches, *Phys. Rev. B* **63**, 054416 (2001).
- <sup>36</sup> A. I. Buzdin, Proximity effects in superconductor-ferromagnet heterostructures, *Rev. Mod. Phys.* **77**, 935–976 (2005).
- <sup>37</sup> J. W. Koo, S. Mitani, T.T. Sasaki, H. Sukegawa, Z.C. Wen, T. Ohkubo, T. Niizeki, K. Inomata and K. Hono, Large perpendicular magnetic anisotropy at Fe/MgO interface, *Appl. Phys. Lett.* **103**, 192401 (2013).
- <sup>38</sup> C.H. Lambert, A. Rajanikanth, T. Hauet, S. Mangin, E.E. Fullerton and S. Andrieu, Quantifying perpendicular magnetic anisotropy at the FeMgO(001) interface, *Appl. Phys. Lett.* **102**, 122410 (2013).
- <sup>39</sup> M. Houzet and A. I. Buzdin, Long range triplet Josephson effect through a ferromagnetic trilayer, *Phys. Rev. B* **76**, 060504 (2007).
- <sup>40</sup> F. S. Bergeret, A. F. Volkov, and K. B. Efetov, Odd Triplet Superconductivity and Related Phenomena in Superconductor-Ferromagnet Structures, *Rev. Mod. Phys.* **77**, 1321 (2005).
- <sup>41</sup> F. Greullet, C. Tiusan, F. Montaigne, M. Hehn, D. Halley, O. Bengone, M. Bowen and W. Weber, Evidence of a Symmetry-Dependent Metallic Barrier in Fully Epitaxial MgO Based Magnetic Tunnel Junctions, *Phys. Rev. Lett.* **99**, 187202 (2007).

## Supplemental material

### Samples description and experimental set-up

The samples were fabricated on single crystal (100) MgO substrates by molecular beam epitaxy in a chamber with  $5 \times 10^{-11}$  mbar base pressure. The substrates were previously degassed by annealing at 600 °C for 20 min before the process. Then, a 10 nm thick seed MgO underlayer was grown at 450 °C on the substrate before the deposition of the other layers, to trap the segregation of any residual carbon impurities. A 2 nm Cr layer is subsequently grown to act as a seed layer for the growth of the next multilayer stack sequences. Then, each layer from the S/F/F and F/S/F junctions stacks (see Fig. 1a,b of the main text) is grown at 100 °C, the metallic layers being later annealed at 450 °C for 20 min to improve their surface and crystalline/epitaxial quality.

The samples were measured inside a Janis  $^3\text{He}$  cryostat with a base temperature of  $T = 0.3$  K. They have attached four contacts each: two for applying current, for which a Keithley 220 current source was used, and two for measuring voltage with a DM-552 voltmeter card integrated into the computer that controls the experiments. Several current sweeps were performed while measuring voltage in order to reduce extrinsic noise sources, and the results were averaged and differentiated to obtain the conductance.

All of the conductance vs bias measurements taken at  $T = 0.3$  K were performed in equilibrium conditions (i.e. with a constant base temperature). However, for the CAs amplitude vs temperature data shown in Figures 2b and 4b in the main text, the method was different. These experiments were made by initially heating the samples up to  $\sim 15$  K and then letting the system to slowly cool down, with a rate of about 1 K/h. During this cooling process, the  $G(V)$  curves were measured, each of them lasting around 1 h, with the temperature measured at the beginning of each curve. Due to this process, the measured temperature as shown in the figures could be overestimated by up to 0.5 K.

### Analysis methods

The conductance anomalies presented in the main text for 3 samples (two S/F/F junctions and an F/S/F one) are widely reproducible in most of the samples of the same lateral sizes that we have studied. Figures 5 and 6 show more examples of junctions of the two types presenting the same periodic features in the above-gap conductance.

For each sample studied, its conductance curve had to be processed to systematically find all the relevant peaks, distinguishing them from the superconducting gap and noisy features. This involved a first step where we ob-

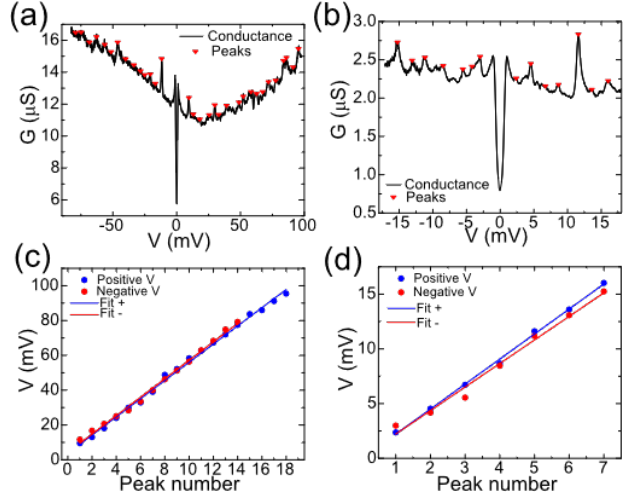


FIG. 5: Conductance curves for two S/F/F junctions, with  $20 \times 20 \mu\text{m}^2$  (a) and  $10 \times 10 \mu\text{m}^2$  (b) lateral dimensions, at  $T = 0.3$  K. Panels (c) and (d) show the analysis of the periodicity of the CAs for the conductance curve shown above each one respectively.

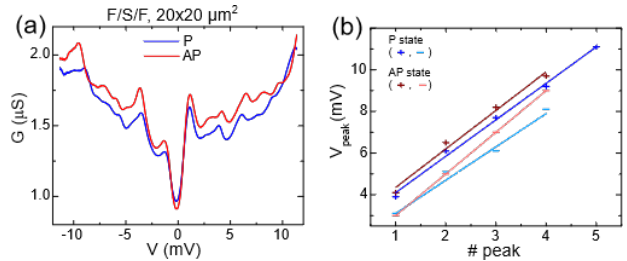


FIG. 6: (a) Conductance curves for a F/S/F junction with  $20 \times 20 \mu\text{m}^2$  lateral dimensions, at  $T = 0.3$  K, in the parallel (P) and antiparallel (AP) configurations of the two F layers. It's worth noting that the gap is deeper in the AP state, due to the reduced effective field from the two surrounding F layers acting on the superconductor. (b) bias position of the above-gap conductance peaks vs peak number for positive and negative applied bias, represented with + and - symbols respectively, and in both magnetic configurations (dark and light blue for the parallel, dark and light red for the antiparallel).

tained a smoothed or “featureless” curve, which was subtracted from the original one to remove the background trend. Once this was done, a simple peak-detecting function could be used in the desired range to find all of the relevant conductance peaks. A threshold was set for the minimum peak amplitude and voltage distance between peaks to avoid noisy features resulting in multiple detections. The results are shown in Figures 5 and 6.

In order to determine the conductance height (ampli-

tude) of each individual CA, a background conductance is subtracted by simply taking two points at each side of the studied peak (where the conductance was already flat), calculating the line that passes through them, and subtracting that baseline from the conductance in the peak range. Then, a fit to a Gaussian function was performed using the non-linear least squares method with a trust region algorithm. The peak amplitude is taken as the height of this Gaussian. Error bars mark the 95% confidence bounds.

## Extended discussion

### Fermi velocity estimation

Based on equation 1 in the main text and the linear fits performed for the bias of the resonance peaks for different samples, an estimation of the Fermi velocity in the Fe layer can be obtained. If  $m$  is the slope of the fit, then the Fermi velocity can be expressed as:

$$v_F^{\text{Fe}} = 4t_{\text{Fe}} \cdot m/h, \quad (2)$$

Where to obtain the velocity in the correct units one has to multiply by the electron charge. The result is a Fermi velocity for the Fe layer of between  $1.93 \times 10^6$  and  $4.83 \times 10^6$  cm/s depending on the studied sample, which is somewhat low compared to tabulated values in the literature<sup>1</sup>. However, there are several reasons which could account for this low value.

### Tomasch vs MacMillan resonances

First, different processes that could also result in peaks or oscillations in the conductance, such as Tomasch reflections<sup>2</sup> or quantum well states, would affect our analysis process by introducing extra peak detections in the conductance curves under study. This means that there is less distance in bias between detected peaks than it should be expected with the contribution from MRRs alone, i.e. a lower slope in eq. 2, which results in an apparent lower  $v_F$ . Nonetheless, it is worth noting that the bias for the oscillations produced by Tomasch reflections is:

$$V_n = \sqrt{\Delta^2 + (nhv_F^S/2d_S)^2}, \quad (3)$$

where  $\Delta$  is the superconducting gap energy,  $h$  the Planck constant,  $v_F^S$  the fermi velocity in the superconducting layer, and  $d_S$  its thickness. This formula is not linear in the low bias regime (for biases of about the

same order of magnitude as the superconducting gap), and we don't see this deviation from a linear trend at low bias. Therefore we rule out these reflections to be the main responsible for the observed CAs in our junctions, although as stated above a small contribution could be present introducing some extra CAs.

Second, the small thickness of the layer makes the transport behavior diverge from that of the bulk. In the same line, the presence of the two MgO electrodes also affects the electronic transport, since the MgO filters out some of the  $k$ -vectors and different electronic symmetries present at the Fe Fermi level<sup>3</sup>. In particular, the  $\Delta_1$  symmetry is the most easily transmitted through the MgO barrier. Since such electrons carry less momentum on average, one could expect to have a relatively low corresponding electronic velocity. Finally, the apparently lower Fermi velocity than expected in bulk Fe could be at least in part caused by the phase delay during the Andreev reflection process as the particle and hole amplitudes penetrate into the superconductor<sup>4</sup>.

### The role of spin-orbit coupling on transport: *dips vs peaks*.

It is also worth mentioning that, in previous observations of McMillan-Rowell resonances due to Andreev reflections in N/S<sup>5,6</sup> or F/S junctions<sup>7,8</sup>, the conductance anomalies usually appeared as periodic peaks in the differential resistance ( $dV/dI$ ), or conversely dips in the differential conductance ( $dI/dV$ ). In contrast, the CAs in our V/MgO/Fe-based junctions look closer to periodic peaks in the differential conductance. We attribute this difference to the critical role that Rashba SOC plays at the MgO/Fe interface in these junctions<sup>3</sup>: Due to the electronic symmetry character of the bands near the Fermi level in Fe(100), only electrons (holes) with  $\Delta_1$  symmetry are transmitted from the V(100) electrode and therefore contribute to the Andreev reflection process. However, this symmetry is absent near the vanadium Fermi level. The presence of interfacial SOC allows for the conversion of  $\Delta_2$  electrons into  $\Delta_1$  (and vice-versa) as well as spin-flip events, making possible the Andreev reflection and therefore the transmission through the MgO barrier (along with quasiparticle penetration into the vanadium in the superconducting state) only for the electrons that have previously suffered SOC scattering. The electrons confined in the Fe electrode, which suffer multiple reflections before penetrating into the superconductor, would therefore have a strongly enhanced probability of undergoing SOC and being transmitted, resulting in a conductance peak instead of the conductance dips observed in heterostructures where SOC does not affect the conductance.



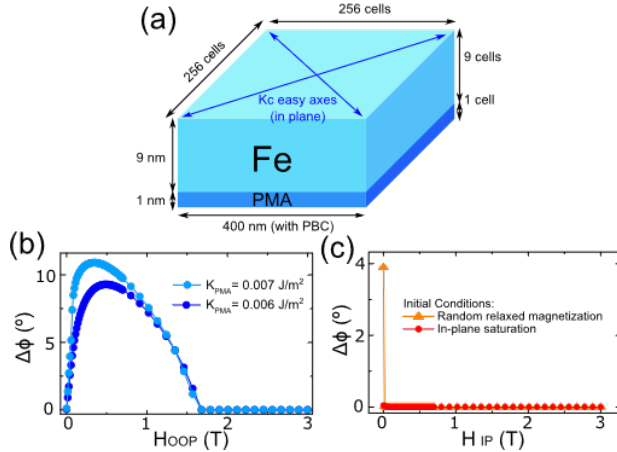


FIG. 7: (a) Sketch of the system simulated in MuMax3 to study the magnetization dynamics of the Fe layer in our junctions under IP and OOP applied fields. (b) Magnetization angle difference between the interfacial layers with PMA and the inner ones vs OOP applied field, for two values of the PMA strength parameter, showing that the behavior is qualitatively robust to variations of the chosen PMA as long as it is present. (c) the same angle difference vs IP applied field, with an initial random relaxed magnetization and with an initial IP saturation.

### Micromagnetic simulations

Micromagnetic simulations were performed using the MuMax3 software<sup>9</sup> in a thin ferromagnetic layer with

PMA under the effect of an OOP magnetic field, as sketched in Figure 7a. As seen in Figure 7b and c, the behavior of the spin textures (measured as the magnetization angle difference between the interfacial and inner layers) is qualitatively similar to the experimental results for the S/F/F junctions: a small applied IP field quickly saturates the magnetization when the initial state is a random magnetization. On the other hand, interfacial spin textures are absent when the magnetization is initially saturated by a 0.1 T field (the experiments were done with an initial IP saturation). However, an OOP field first induces a maximum angle difference before saturating the magnetization under a sufficiently high OOP field. The parameters used for the simulated Fe were a damping parameter  $\alpha = 0.02$ ; saturation magnetization  $M_{\text{sat}} = 1.7$  T; an exchange stiffness constant  $A_{\text{ex}} = 21 \times 10^{-12}$  J/m; a cubic anisotropy  $K_C = 4.8 \times 10^4$  J/m<sup>3</sup>; with a number of cells equal to  $N_X = N_Y = 256$ ;  $N_Z = 10$  corresponding to dimensions  $L_X = L_Y = 400$  nm;  $L_Z = 10$  nm. The PMA was set as an uniaxial anisotropy in the OOP direction with anisotropy constant  $K_U = K_{\text{PMA}} \times N_Z/L_Z$ , which is shown in Figure 7b for two different strengths to prove that the observed behavior is qualitatively robust and not a result of fine-tuning.

\* e-mail: farkhad.aliev@uam.es

<sup>1</sup> N. W. Ashcroft and N. D. Mermin, Solid State Physics, Saunders, 1976.

<sup>2</sup> W. L. McMillan and P. W. Anderson, Theory of geometrical resonances in the tunneling characteristics of thick films of superconductors, Phys. Rev. Lett. **16**, 85–87 (1966).

<sup>3</sup> I. Martínez, P. Högl, C. González-Ruano, J. P. Cascales, C. Tiusan, Y. Lu, M. Hehn, A. Matos-Abiague, J. Fabian, I. Zutic and F. G. Aliev, Interfacial Spin-Orbit Coupling: A Platform for Superconducting Spintronics, Phys. Rev. Applied **13**, 014030 (2020).

<sup>4</sup> M. Eschrig, Spin-polarized supercurrents for spintronics: a review of current progress, Rep. Prog. Phys. **78**, 104501 (2015).

<sup>5</sup> H. S. Chang, M. H. Bae, and H. J. Lee, McMillan–Rowell oscillations observed in c-axis Au/Bi<sub>2</sub>Sr<sub>2</sub>CaCu<sub>2</sub>O<sub>8+δ</sub> junctions, Physica C **408-410**, 618-619 (2004).

<sup>6</sup> O. Neshor and G. Koren, Measurements of

$\Delta$  and  $v_F$  from Andreev reflections and McMillan-Rowell oscillations in edge junctions of YBa<sub>2</sub>Cu<sub>3</sub>O<sub>6.6</sub>/YBa<sub>2</sub>Cu<sub>2.55</sub>Fe<sub>0.45</sub>O<sub>y</sub>/YBa<sub>2</sub>Cu<sub>3</sub>O<sub>6.6</sub>, Physical Review B **60**, 9287 (1999).

<sup>7</sup> C. Visani, Z. Sefrioui, J. Tornos, C. Leon, J. Briatico, M. Bibes, A. Barthélémy, J. Santamaría and J. E. Villegas, Equal-spin Andreev reflection and long-range coherent transport in high-temperature superconductor/half-metallic ferromagnet junctions Nature Physics **8**, 539–543 (2012).

<sup>8</sup> C. Visani, F. Cuellar, A. Pérez-Muñoz, Z. Sefrioui, C. León, J. Santamaría and J. E. Villegas, Magnetic field influence on the proximity effect at YBa<sub>2</sub>Cu<sub>3</sub>O<sub>7</sub>/La<sub>2/3</sub>Ca<sub>1/3</sub>MnO<sub>3</sub> superconductor/half-metal Phys. Rev. B **92**, 014519 (2015).

<sup>9</sup> A. Vansteenkiste et. al; The design and verification of MuMax3, AIP Advances **4**, 107133 (2014).